Q_y-Level Structure and Dynamics of Solubilized Light-Harvesting Complex II of Green Plants: Pressure and Hole Burning Studies

J. Pieper,[†,‡] M. Rätsep,[‡] R. Jankowiak,[‡] K.-D. Irrgang,[§] J. Voigt,[†] G. Renger,[§] and G. J. Small*[,‡]

Institute of Physics, Humboldt University, 10099 Berlin, Germany, Ames Laboratory—U.S. Department of Energy and Department of Chemistry, Iowa State University, Ames, Iowa 50011, and Max-Volmer Institute, Technical University, 10623 Berlin, Germany

Received: October 5, 1998; In Final Form: December 10, 1998

Nonphotochemical hole burning and pressure-dependent absorption and hole-burning results are presented for the isolated (disaggregated) chlorophyll *a*/*b* light-harvesting II trimer antenna complex of green plants. Analysis of the 4.2 K burn-fluence dependent hole spectra and zero-phonon hole action spectra indicates that the three lowest energy states (Q_y) lie at 677.1, 678.4 and 679.8 nm. Their combined absorption intensity is equivalent to that of three Chl *a* molecules. The inhomogeneous broadening of their absorption bands is 70 cm^{-1}. It is argued that these states, separated by 30 cm^{-1}, are associated with the lowest energy state of the trimer subunit with the 30 cm^{-1} separations due to the indigenous structural heterogeneity of protein complexes. The linear electron−phonon coupling of the 679.8 nm state is weak and characterized, in part, by a mean phonon frequency of $\omega_m = 18$ cm^{-1} and Huang−Rhys factor of $S_m = 0.8$, values which yield the correct Stokes shift for fluorescence from the 679.8 nm state at 4.2 K. The temperature dependence of the zero-phonon hole (ZPH) width for that state is consistent with optical dynamics due to coupling with glasslike two-level systems of the protein. The ZPH width at 1.9 K is 0.037 cm^{-1}. Satellite hole structure produced by burning in the above three states as well as their low linear pressures shift rates (about − 0.08 cm^{-1}/MPa) indicate that the Chl *a* molecule of the subunit associated with them is weakly coupled to other Chl molecules. The linear pressure shift rates for the main Q_y-absorption bands are also low. The shift rates appear to be dictated by protein−Chl interactions rather than excitonic couplings. Holes burned into the 650 nm absorption band reveal energy transfer times of 1 ps and ∼100 fs which are discussed in terms of time domain measurements of the Chl *b* → Chl *a* transfer rates (Connelly et al. *J. Phys. Chem. B* **1997**, *101*, 1902). The holewidths associated with burning into the 676 nm absorption band lead to Chl *a* → Chl *a* transfer times in the 6−10 ps range, in good agreement with the time domain values (Savikhin et al. *Biophys. J.* **1994**, *66*, 1597).

1. Introduction

Photosynthetic antenna systems are most often comprised of two or more protein−chlorophyll (Chl) complexes whose excited state (Q_y) electronic structures and spatial arrangement around the reaction center complex serve to efficiently transfer solar excitation energy to the special pair (primary electron donor) of the reaction center (for reviews see refs 1−4). A firm understanding of excitation energy transfer (EET) between and within complexes requires, in addition to their structures, an accurate description of the Q_y-excited electronic states, the inhomogeneous and homogeneous broadenings of Q_y-absorption bands, the distribution of donor (D)−acceptor (A) state energy gaps which stem from the intrinsic heterogeneity of proteins or symmetry/chemical inequivalence of the Chl molecules, and electron−vibration and *N*-phonon couplings.

In higher plants and green algae the Chl *a*/*b* light-harvesting complex II (LHC II) associated with photosystem II is the most abundant and is located peripherally to the reaction center (for a review see ref 5). The determination of its structure to a resolution of 3.4 Å[6] has led to a number of ultrafast[7−12] and frequency domain[13−16] studies of LHC II's EET processes and electronic structure. The LHC II protein crystallizes as a C_3 trimer of subunits, each of which contain 12 Chl molecule arranged in two layers close to the upper and lower surfaces of the membrane with the planes of the macrocycles close to perpendicular to the membrane plane. Except for the possibility that two of the Chl molecules of the subunit are related by diad symmetry, the pigments appear to be symmetry inequivalent. Within each of the two layers the shortest $R_{Mg\cdots Mg}$ distances are in the range of ∼9−14 Å. The 3.4 Å resolution map does not allow for distinction between Chl *a* and *b* molecules or determination of their Q_y-transition dipole directions. However, an assignment of the seven Chl *a* molecules was made on the basis of the physiological criterion of efficient triplet state quenching of Chl *a* molecules by the carotenoid molecules of the subunit.[6] With this assignment, $R_{Mg\cdots Mg}$ distances for five pairs of Chl *a* and Chl *b* molecules fall in the range of 8.3−10.5 Å. (The shortest Chl *a*−Chl *a* and Chl *b*−Chl *b* distances are ∼11 Å.) The shortest interatomic distances are 4.0−5.0 Å. (The uncertainty in the distances is ∼1 Å). Such distances suggest the possibility of relatively strong electrostatic or even electron-exchange coupling between the Chl *a* and *b* molecules of the pairs.

The 4.2 K absorption spectrum of the LHC II trimer is shown in Figure 1. On the basis of the absorption spectra of Chl *a* and *b* monomers in solution, there is general agreement that the

† Institute of Physics.
‡ Ames Laboratory.
§ Max-Volmer Institute.
* Corresponding author.

10.1021/jp983957l CCC: $18.00
Published on Web 02/20/1999

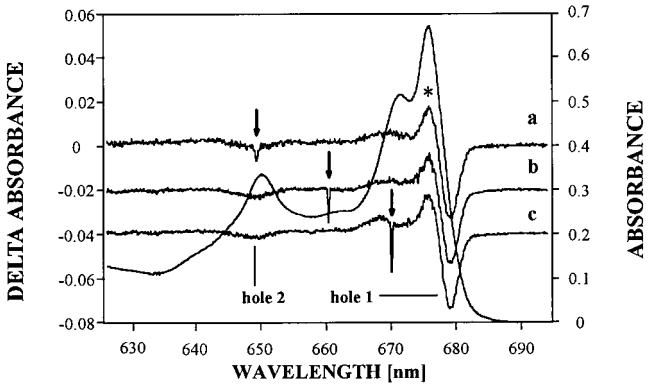

Figure 1. The 4.2 K absorption spectrum of the LHC II trimer with principal bands at 676.1, 671.3, 661.4, and 649.5 nm; absorbance is given by the right vertical scale. Also shown are three hole-burned spectra obtained with burn wavelengths indicated by the arrows, a burn fluence of 78 J/cm^2, and a read resolution of 4 cm^{-1}. Spectrum a is twice enlarged. The feature indicated by the asterisk is the antihole of hole 1.

absorptions at 650 nm and ~670−680 nm are mainly due to Chl *b* and *a*, respectively. The first detailed investigation of the Q_y-structure of the LHC II trimer was made on the basis of 77 K absorption, linear dichroism, and circular dichroism spectra.[13] Nine states were assigned in the region between ~650 and 676 nm. The results indicated the existence of significant and complex excitonic couplings. The lowest energy state was assigned at 676 nm, the position of the most intense absorption band. Later, zero-phonon hole (ZPH) action spectroscopy at 4.2 K led to the assignment of the lowest energy state to a relatively weak transition at ~680 nm[15] which exhibits coupling to phonons of mean frequency $\omega_m = 20$ cm^{-1} with a Huang−Rhys factor of $S_m = \sim 0.4-0.5$. With the lowest energy state at 680 nm and an optical reorganization energy of $S_m\omega_m = 8$ cm^{-1}, the 6 nm red shift of the fluorescence origin band relative to the 676 nm absorption band was reasonably well accounted for. Subsequently, triplet−singlet absorption spectroscopy[17] and fluorescence line narrowing and temperature-dependent absorption spectroscopies[16] were used to confirm the existence of a 680 nm state whose absorption, we note, is not resolved from that of the 676 nm band in Figure 1. The results of 77 K[12] and 12 K[11] femtosecond transient absorption measurements are consistent with the existence of a 680 nm state.

Several femtosecond spectroscopic studies with excitation near 650 nm have been reported on during the last five years.[7−12] As discussed in ref 7, Chl *b* → Chl *a* EET occurs with kinetic components of ~150 fs, 600 fs, and 10 ps. These kinetics appear to be weakly temperature dependent. Results obtained for the subunit of the LHC II trimer indicate that these transfer processes occur within the subunit,[18] consistent with the large distances and concomitant weak couplings between Chl molecules belonging to different subunits.[19] Energy transfer/equilibration associated with states that contribute to the 670 and 676 nm absorption band occurs on a time scale of ~10−20 ps.[8] These kinetics are also weakly dependent on temperature.

A detailed understanding of the EET dynamics of the LHC II trimer requires an accurate description of the Q_y-states which, in turn, requires a diffraction map of high enough resolution to distinguish between the Chl *a* and *b* molecules, define the directions of the Q_y-transition dipoles and provide intermolecular and interatomic distances accurate to a couple tenths of an angstrom. However, valuable insights can be gained by modeling time and frequency domain spectroscopic data under the constraints imposed by the current 3.4 Å resolution structure. Work in this direction has recently begun. With the aforementioned Chl *a*/*b* assignments, a complete set of Q_y-transition dipole directions has been proposed.[20] For optimal mutual orientations, the maximum excitonic coupling for neighboring Chl *a* and *b* molecules is estimated to be ~150 cm^{-1} with $\epsilon = 1$[21,22] while Chl *a*−Chl *a* couplings appear to be considerably weaker. Possible alignments of the two Q_y-transition dipoles associated with the optimal orientations of Chl *a* and *b* pairs is considered in ref 12. Because the 150 cm^{-1} coupling is small relative to Chl *b*−Chl *a* energy gap of ~600 cm^{-1}, it was found that excitonic interactions between Chl molecules have a small effect on the Q_y-energies although they result in significant redistribution of oscillator strengths.[21,22] It appears from that work that protein−Chl interactions are more important than excitonic interactions in determination of the Q_y-energies. The question of whether Förster theory can be applied to the ultrafast Chl *b* → Chl *a* energy transfer processes was raised in ref 9 and considered further in refs 19 and 22. That is, it is possible that transfer need be formulated in terms of zero-order wave functions that are excitonic (eigenstates of a Hamiltonian that contains the static intermolecular potential) rather than wave functions localized on individual Chl molecules. The model calculations presented in refs 12 and 23 assume that the Förster picture is applicable.

The persistent nonphotochemical hole-burning (NPHB) experiments reported on here were more detailed and of higher resolution than those of Reddy et al.[15] Furthermore, aggregation of trimers in the samples used was reduced as will be shown in the accompanying paper.[24] Attention is focused on (i) identification and characterization of the states in the near vicinity of 680 nm, (ii) the electron−phonon coupling of those and other states, (iii) the optical dynamics of the lowest energy state which lies at 679.8 nm, and (iv) the EET dynamics of states associated with the 650 and 676 nm bands. In addition, the first high-pressure absorption and hole-burning results for the LHC II trimer are presented and discussed in terms of excitonic coupling and protein−Chl interactions. Utilization of pressure has been shown to be a useful approach for gauging the strength and nature of Chl−Chl interactions.[25,26] By way of background on those attributes of NPHB which are relevant to i−iv, we note first that NPHB has been used to determine the inhomogeneous and homogeneous broadenings of the Q_y-absorption bands of many photosynthetic complexes (for reviews see refs 27 and 28). (Recent results from ultrafast experiments indicate that inhomogeneous broadening is as important at biological temperatures as it is at liquid helium temperatures.[29−31]) Furthermore, it was found that D−A state energy gaps of chemically identical complexes in a bulk sample are largely uncorrelated, which means that one is confronted with a distribution of gap values which, if sufficiently wide, can lead to dispersive kinetics for D → A transfer.[32] There are no other results than those from NPHB that directly establish this. Concerning the linear electron−phonon coupling strengths of antenna $S_1(Q_y) \leftarrow S_0$ ground state absorption transitions, NPHB has shown that they are weak and mainly associated with protein−Chl intermolecular modes with frequencies in the ~20−30 cm^{-1} range and Huang−Rhys factors (S) $\lesssim 1$. The Huang−Rhys factors enter into the EET rate expressions and are also important for assessing whether the exciton−phonon interaction leads to self-trapping of the exciton in systems where the Q_y-states are delocalized.[33] Exciton level structure of antenna complexes characterized by strong ($\gtrsim$100 cm^{-1}) Chl−Chl couplings can also be studied by NPHB. The LH2 (B800-850) and LH1 (B875) light harvesting (LH) complexes of purple bacteria serve as good examples. For

example, ZPH action spectroscopy led to identification and characterization of the lowest energy and weakly absorbing exciton level (A symmetry) of the cyclic B850 ring of BChl *a* dimers for three species[34−36] as well as the corresponding A level of the B875 ring of *Rhodobacter sphaeroides*.[25] The location of the A level can serve as a benchmark for electronic structure calculations. It was also found that[37] the B850 and B875 absorption bands are significantly homogeneously broadened. The broadening was attributed to ultrafast (∼100 fs) interexciton level relaxation via the Davydov mechanism.[38] Low-temperature femtosecond pump−probe experiments later provided more detail on the ultrafast relaxation processes.[29,31,39] The cyclic symmetries of the B850 and B875 rings lead to considerable simplification in determination of their exciton level structures and the effects of energy disorder (diagonal and/or off-diagonal) on the levels.[40,41] In contrast, the BChl *a* (FMO) antenna complex of the green bacteria *Prosthecochloris aestuarii*[42] and *Chlorobium tepidum*,[43] which has more in common with the LHC II complex of photosystem II, exhibits only the C_3 symmetry that relates the three subunits of the complex. Each subunit contains seven symmetry and energetically inequivalent BChl *a* molecules with nearest neighbor distances (Mg···Mg) in the range 11.3−14.4 Å and coupling energies as large as ∼150 cm^{-1}. (The strongest pairwise interaction between BChl *a* molecules belonging to different subunits is ∼15 cm^{-1}.) The symmetry inequivalence leads to uncertainty in theoretical modeling of the exciton level structure of the trimer.[44−46] Nevertheless, it appears that the Q_y-states are miniexcitons with excitation shared by no more than approximately three BChl *a* molecules of the subunit and that the lowest energy state of the subunit is mainly localized on a single BChl *a* molecule. The lowest energy state is responsible for the 825 nm absorption band which hole burning had revealed is contributed to by at least two levels at 824 and 827 nm.[47] The assignment favored in that work was that the two levels are the A and E levels of the trimer associated with the lowest energy state of the subunit. On the basis of recent work on the localization of exciton levels produced by energy disorder, it seems more likely that the two levels represent excitations localized mainly on different subunits of the trimer.[41,45] It is argued here that this type of situation most likely exists for the LHC II trimer.

2. Materials and Methods

Sample Preparation. LHC II preparations were isolated by solubilization of salt washed PS II membrane fragments of spinach in the presence of β-dodecyl maltoside (DM) and separation by sucrose density gradient centrifugation as described in ref 48. The Q_y-absorption spectrum at room temperature exhibited two bands with maxima at 652 ± nm and 675 ± 1 nm. The room-temperature CD spectrum was identical to that of the trimer complex shown in ref 49. A Chl *a*/Chl *b* ratio of 1.35 ± 0.05 was determined using the method of Porra et al.[50] Polypeptide analysis using the PAGE procedure of Irrgang et al.[48] revealed the presence of the minor Chl *a*/Chl *b* binding proteins CP14/15, CP22, CP24, and CP26 (see ref 51). The samples were diluted with a glass forming buffer solution containing 0.025% w/v β-DM and 70% w/v glycerol as the glass forming solvent. This solvent composition minimizes undesirable aggregation of the LHC II trimer as discussed in ref 52. The total Chl concentration of samples used for hole burning and fluorescence measurements was 0.007 and 0.200 mg/mL, respectively.

Spectroscopic Methods. The hole-burning apparatus is described in detail elsewhere.[53] Briefly, the burn laser was a Coherent CR 699-21 dye laser (line width of ∼0.05 cm^{-1}) pumped by a 6 W Coherent Innova Ar ion laser. The sample temperature was maintained at 4.2 K using a Janis 8-DT convection cooling liquid helium cryostat. Burn fluences or burn intensities (I_B) and times (τ_B) are given in the figure captions. A Bruker IFS 120 HR Fourier transform spectrometer was used to record (read) the preburn and postburn absorption spectra. A read resolution of 0.3 cm^{-1} was used in determination of the zero-phonon hole (ZPH) widths reported. A resolution of 4 cm^{-1} was otherwise used.

The high-pressure apparatus has been described in detail in refs 54 and 55, including the procedure used to measure pressure. To ensure good optical quality, the sample was contained in a gelatin capsule (5 mm outside diameter) and then housed in a specially designed high pressure cell with four sapphire windows (thickness of 4 mm) providing optical access. The cell was connected to a three-stage hydraulic compressor (Model U11, Unipress Equipment Division, Polish Academy of Sciences) through a flexible thick-walled capillary (o.d./i.d. = 3.0 mm/0.3 mm). Helium gas was used as the pressure-transmitting medium. A specially designed Janis 11-DT cryostat was used for cooling of the high-pressure cell. High-pressure hole burning was performed at 12 K. At this temperature liquid helium solidifies at ∼75 MPa. Following the procedure given in ref 54, it was confirmed that pressure-induced structural changes are elastic. For studies at higher temperatures, a Lakeshore temperature controller (model 330) was used to stabilize the temperature. After the diode reading reached the pre-set temperature, the sample was allowed to equilibrate for 15 min prior to initiating absorption or hole-burning measurements.

A N_2-laser pumped dye laser (Laser Sci Inc. VSL-Dye) of 3 ns pulse duration and repetition rate of 20 Hz was used as the excitation source for the fluorescence measurements. Samples were excited at 430 nm with pulse energies of about 10^{13} photons/cm^2. Fluorescence spectra were measured using a double monochromator (Carl Zeis Jena, GDM 1000) at a resolution of 0.5 nm with an avalanche diode detector (type 712-A4). Samples were contained in 0.01 mm cuvette at 4.2 K. An optical density of 0.02 at 676 nm ensured that reabsorption effects were negligible.

3. Results

Hole-Burning Results at Ambient Pressure. The 4.2 K absorption spectrum of Figure 1 is similar to that reported by Reddy et al.[15] with four partially resolved bands at 676.1, 671.3, 661.4, and 649.5 nm. Hole-burned spectra were obtained with burn wavelengths (λ_B) between 640 and 684 nm. The ZPH burning efficiencies for 660 nm $\lesssim \lambda_B \lesssim$ 674 nm were found to be about an order of magnitude lower than for $\lambda_B \gtrsim$ 675 nm. The efficiencies for 640 nm $\lesssim \lambda_B \lesssim$ 655 nm were still lower, by about a factor of 5. The decrease in efficiency with decreasing λ_B is qualitatively consistent with an increase in the EET rate with decreasing wavelength since the hole-burning efficiency is determined, in part, by the induced absorption rate of the zero-phonon line which is inversely proportional to the total optical dephasing time T_2.[56,57,58] We recall that $T_2^{-1} = (2T_1)^{-1} + T_2^{*-1}$, where T_1 would be the inverse of the EET rate and T_2^* the pure dephasing time. For EET rates higher than $(10\ ps)^{-1}$, the pure dephasing time is expected to be negligible at 4.2 K.[56]

The hole-burned spectra a, b, and c of Figure 1 were obtained with λ_B = 648.6, 660.0, and 670.0 nm, respectively, and show structure that is typical of spectra obtained with 640 nm $\lesssim \lambda_B \lesssim$ 674 nm. First, there is the ZPH coincident with λ_B which is

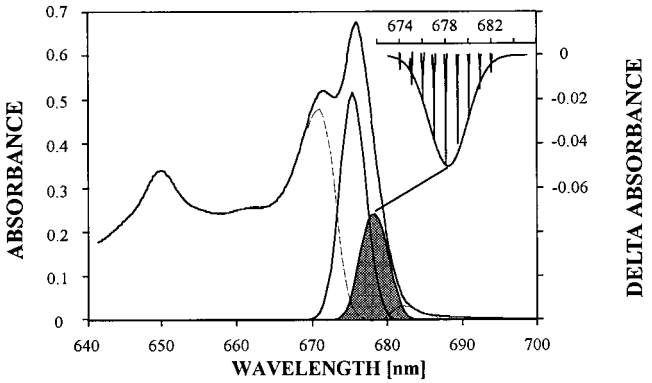

Figure 2. The zero-phonon hole action spectrum (inset) of LHC II trimer obtained with burn wavelengths in the vicinity of 680 nm and a constant burn fluence of 3.6 J/cm^2. The profile of the action spectrum is approximately Gaussian with a width of 85 cm^{-1}. It is also depicted by the hatched profile to the right of the 676 nm absorption band. See Discussion section for deconvolution procedure used to determine that the absorption intensity of the three lowest energy states associated with the action spectrum is equivalent to that of ~3 Chl *a* molecules. For convenience the absorption spectrum from Figure 1 is also shown.

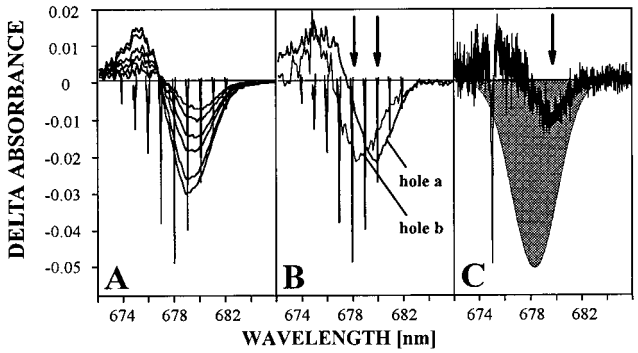

Figure 3. Frame A: Burn fluence dependence of hole 1 (Figure 1) obtained for $\lambda_B = 660$ nm, a burn intensity of 130 mW/cm^2 and burn times (top to bottom) of 1, 2, 5, 10, 20, and 30 min. Read resolution = 4.0 cm^{-1}. The ZPH action spectrum of Figure 2 is shown for comparison. Frame B: Further illustration of the blue shift of hole 1. Hole a was obtained for the shortest burn time of 30 s while hole b is the difference between the low two hole spectra of frame A. Holes a and b peak at 679.8 ± 0.2 and 678.4 ± 0.2 nm (see arrows). Frame C: Hole spectrum obtained with $\lambda_B = 675.0$ nm (coincident with the sharp ZPH), burn intensity = 100 mW/cm^2, and burn time = 60 s. The broad hole indicated by the arrow at 679.8 nm carries a width of 70 cm^{-1}, see text. For convenience the profile of the action spectrum is shown.

indicated by an arrow. Second, there is a broad hole near 680 nm which is labeled as hole 1. Third, there is a broad hole near 648 nm with a width of ~125 cm^{-1}, labeled as hole 2, which is close to the maximum of the 650 nm absorption band. The positive feature labeled by the asterisk is the blue-shifted anti hole of hole 1. These general features have previously been observed.[15] As discussed in that work, hole 1 is due to hole burning in a state(s) near 680 nm which is rapidly populated by EET from higher states excited by the burn frequency. (NPHB rates are typically much slower than (1 ns)$^{-1}$.[59]) The inset of Figure 2 shows the ZPH action spectrum obtained with constant burn fluence of 3.6 J/cm^2 and λ_B-values in the vicinity of 680 nm. The read resolution used was 0.3 cm^{-1}, which is an order of magnitude higher than used in ref 15. The action spectrum establishes that hole 1 of Figure 1 is inhomogeneously broadened and, furthermore, that the site excitation energy distribution function (SDF) of the state(s) near 680 nm is largely uncorrelated with those of the higher energy states. The action spectrum is approximately Gaussian with a width (fwhm) of 85 ± 10 cm^{-1} and is centered at 678.2 ± 0.2 nm, which is 1.3 nm lower than the value reported by Reddy et al.[15] The ZPH widths (uncorrected for read resolution) range from 2.5 cm^{-1} for $\lambda_B = 675$ nm to 0.5 cm^{-1} for burn wavelengths between 679 and 682 nm. These holewidths as well as those of the broad and the relatively sharp hole near 650 nm in the upper spectrum of Figure 1 are discussed in the following section.

The hole spectra of Figure 1 were obtained with a burn fluence of 78 J/cm^2. Hole 1 was centered at 679.3 nm for all λ_B-values $\lesssim$ 674 nm used. The ZPH action spectrum of Figure 2, with a maximum at 678.2 nm, was obtained with a much lower fluence of 3.6 J/cm^2. To investigate the source of the 1.1 nm difference between these two maxima, the dependence of hole 1 on burn fluence was determined. Results are shown in frame A of Figure 3 for $\lambda_B = 660$ nm. (For comparison the ZPH action spectrum from Figure 2 is also shown.) Burn intensities and times for the six spectra of hole 1 are given in the caption. The wavelength of the maximum of hole 1 decreases from 679.8 nm (top profile; burn fluence = 7.8 J/cm^2) to 679.0 nm (bottom profile; burn fluence = 230 J/cm^2). The blue-shifting of hole 1 with increasing burn fluence suggests the presence of at least two states near 680 nm, with one being the terminal and lowest energy (fluorescent) state at 679.8 nm. That is, because the terminal state has a lifetime of a few ns, it undergoes hole burning first since the higher energy state(s) near 678 nm should have a considerably shorter lifetime due to EET. This follows from the theory of persistent hole burning. Part C of Figure 3 shows a hole-burned spectrum obtained with λ_B = 675.03 nm, $I_B = 100$ mW/cm^2, and $\tau_B = 60$ s that provides additional support for the lowest energy state being at 679.8 nm. The broad satellite hole indicated by the arrow is at 679.8 nm. Its width, after a correction for interference from the antihole on the high energy side, is ~70 cm^{-1} which is 15 cm^{-1} narrower than that of the ZPH action spectrum. The shaded gray profile in frame C is the Gaussian profile of the action spectrum. The fractional OD changes at the hole 1 maxima in frame A of Figure 3 are, from top to bottom, 0.040, 0.060, 0.085, 0.11, 0.16, and 0.19. The extent of the blue shifting with increasing burn fluence is more apparent in frame B where hole a was obtained under the conditions used to obtain the results of frame A except that $\tau_B = 30$ s and hole b is the difference between the lowest two profiles of frame A (normalized to the same peak intensity as hole a). The maxima of holes b and a are at 678.4 ± 0.2 nm and 679.8 ± 0.2 nm, respectively, with the former wavelength equal, within experimental uncertainty, to the maximum of the ZPH action profile. The energy separation that corresponds to these two wavelengths is 22 cm^{-1}, which is large relative to *kT* at 4.2 K (2.9 cm^{-1}). Thus, at 4.2 K one expects that most of the fluorescence should originate from the 679.8 nm state. This is relevant to the discussion of the 4.2 K non-line narrowed fluorescence spectrum (Figure 8).

The fractional OD change of the two most intense ZPH of the action spectrum is ~0.16 which is comparable to the changes for the two most intense hole 1 profiles of frame A in Figure 3. That the former and latter were obtained with burn fluences of ~4 and 200 J/cm^2 might, at first sight, appear to be inconsistent. However, this is not the case since the effective *spectral* burn intensity or fluence must be taken into account. For the case of hole 1, the burn fluence of 200 J/cm^2 needs to be multiplied by the ratio of the homogeneous width of the ZPL excited at λ_B = 660 nm (~2 cm^{-1}) divided by the inhomogeneous width of the ZPH action profile (~85 cm^{-1}). This follows since, as previously mentioned, the SDFs of the higher energy states and the state(s) associated with the ZPH action spectrum are uncorrelated. Thus, the excitation energy absorbed in a ~2 cm^{-1} interval

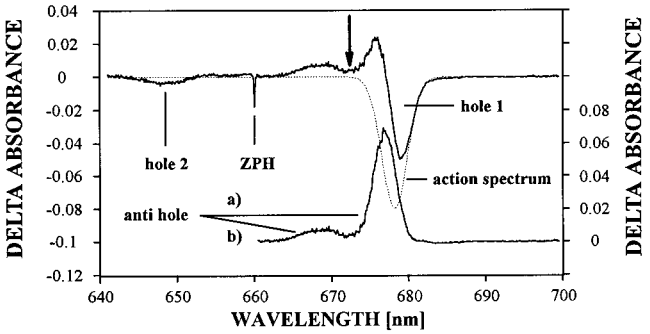

Figure 4. Saturated hole spectrum (top) of LHC II trimer obtained with $\lambda_B = 660.0$ nm (coincident with sharp ZPH), burn intensity = 130 mW/cm^2, and burn time = 30 min. The envelope of the ZPH action spectrum (dashed curve) is fitted to the low energy wing of hole 1. The bottom spectrum is the difference between it and the top spectrum and represents the antihole spectrum, see text.

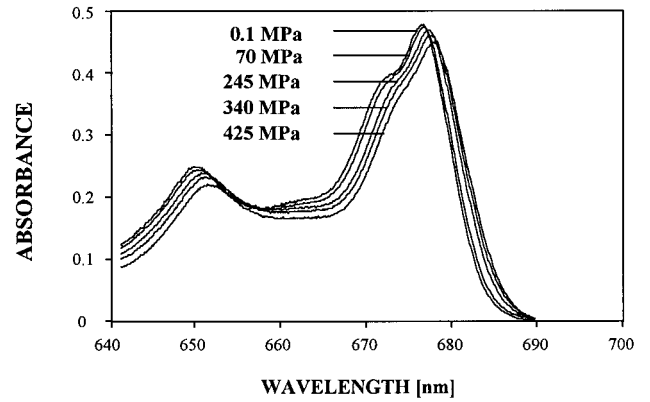

Figure 5. Pressure dependence of LHC II trimer's absorption spectrum at 77 K. Upon pressure release the ambient pressure (0.1 MPa) spectrum was recovered indicating elastic behavior (result not shown).

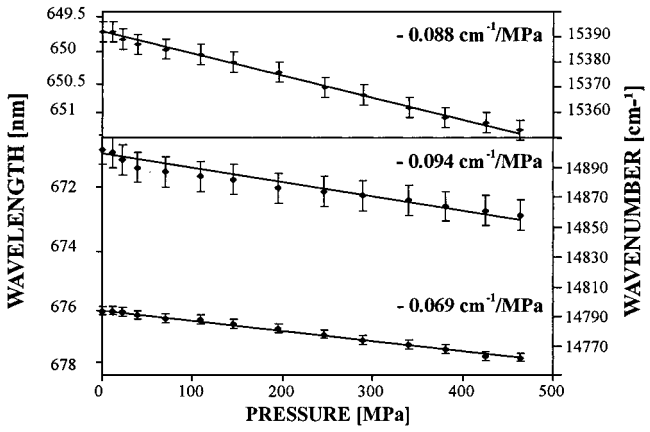

Figure 6. Linear pressure shifting of the 649.5 nm (top), 671.3 nm (middle), and 676.1 nm (bottom) absorption bands of LHC II trimer, 77 K. Shift rates are given in the figure.

at 660 nm is distributed over the inhomogeneously broadened absorption profile of the ~680 nm state(s) prior to hole burning.

In frame A of Figure 3 one can see that the high energy side of hole 1 sharpens as the burn fluence increases. This is the result of interference by the low energy side of the antihole which, it should be noted, also shifts to the blue with increasing burn fluence. The asymmetry of hole 1 is more apparent in the upper spectrum of Figure 4 where it is saturated. The profile of the ZPH action spectrum is shown as the dashed curve. The difference between the upper spectrum and the action spectrum fitted to the low energy side of hole 1 is shown at the bottom and represents the antihole spectrum. Antihole a is symmetric

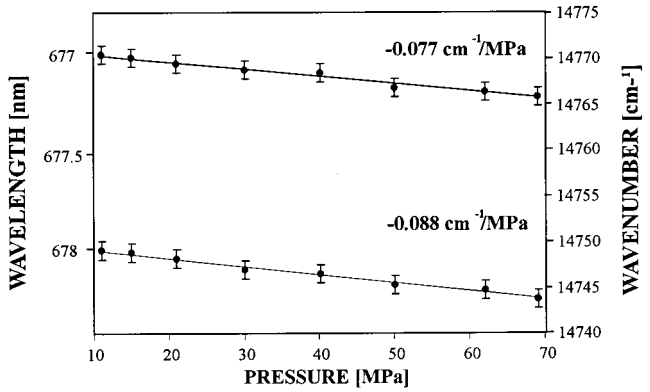

Figure 7. Linear pressure shifting of two zero-phonon holes burned at 677.0 nm (top) and 678.0 nm (bottom), $T = 12$ K. Shift rates are given in the figure.

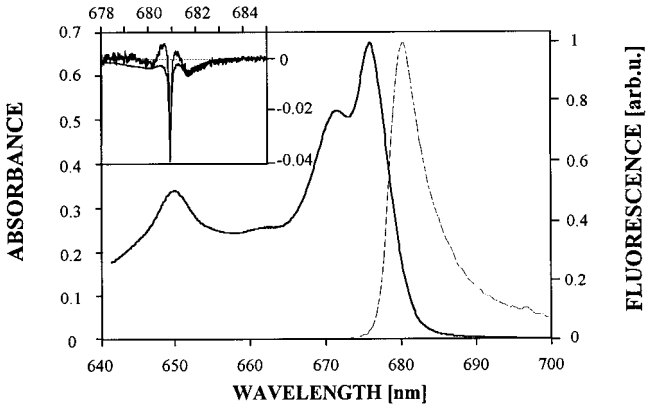

Figure 8. 4.2 K absorption spectrum and nonline narrowed fluorescence origin profile (crosses). The maximum of the fluorescence origin is at 680.3 nm. The inset shows a hole-burned spectrum (noisy) obtained with $\lambda_B = 681.0$ nm, burn intensity = 50 mW/cm^2, and burn time = 300 s. The fractional hole depth of the ZPH at 681.0 nm is 0.36. The theoretical fit was obtained with $S = 0.8$, $\omega_m = 18$ cm^{-1}, and the one-phonon profile defined in the text. The effective burn time was adjusted to account for the depth of the ZPH. Except for the antihole (positive ΔA) region, which the theory does not account for, the fit is satisfactory, see pseudo-phonon sideband hole at 681.7 nm.

with a width of 85 cm^{-1}. It is associated with hole 1, relative to which it is shifted by +25 cm^{-1}. The integrated intensity of antihole a accounts for 80% of the intensity of hole 1. The discrepancy of 20% can be understood in terms of interference of the actual antihole, which typically is asymmetric with tailing to high energy,[60] and the hole indicated by the arrow in the upper spectrum, see also Figure 1. This hole appears to be associated with the 671 nm absorption band. Antihole b is most likely associated with that hole. The sum of the intensities of antiholes a and b equals that of hole 1. Thus, we may conclude that the mechanism of hole burning is nonphotochemical.

We consider next results on linear electron−phonon coupling of LHC II. Of particular interest is the coupling for the lowest energy state at ~679.8 nm, since it is relevant to interpretation of the Stokes shift for the fluorescence origin band, see Discussion section. Earlier hole-burned spectra obtained with λ_B ~681 nm indicated that the coupling to low-frequency intermolecular modes is dominated by protein phonons with mean frequency ω_m ~20 cm^{-1} and S_m ~0.5.[15] As a check on these values we performed more detailed experiments and theoretical analysis. Hole spectra were obtained with $\lambda_B = 681$ nm and $I_B = 50$ mW/cm^2 for burn times between $\tau_B = 30$ and 300 s. The read resolution used was 0.3 cm^{-1}. In the shallow burn limit ($\tau_B = 30$ s), real and pseudo-phonon sideband holes

at $\sim \pm 20$ cm^{-1} relative to the ZPH were observed (results not shown). The theory given in ref 61 was used to fit the spectrum. As input the theory requires values for the center wavelength and width of the zero-phonon line excitation energy profile. The values of 678.2 nm and 85 cm^{-1} from the ZPH action spectrum, Figure 2, were used. A good fit was obtained for $S_m = 0.8$, $\omega_m = 18$ cm^{-1}, and a width of $\sim$25 cm^{-1} for the one-phonon profile. A Gaussian and Lorentzian were used to describe the low and high energy sides of the one-phonon profile with widths (fwhm) of 10 and 40 cm^{-1}, respectively. As discussed in refs 62 and 63, it is important that the parameter values determined from hole-burned spectrum in the shallow burn limit provide a good description of the spectra obtained with higher burn fluences. The inset of Figure 8 shows the $\tau_B = 300$ s spectrum. The fractional OD change of the ZPH is 0.36. The pseudo- and real PSBH are indicated by solid and dashed arrows, respectively. Comparison with the calculated fit should be restricted to the ZPH and the pseudo-PSBH since the antihole, which is not accounted for in the theory, interferes with the real PSBH. The fit accounts for the width and intensity of the ZPH and provides a reasonable description of the pseudo-PSBH. As an independent check on the 0.8 value for S_m it was determined that the fractional OD change for the saturated ZPH at $\lambda_B = 681$ nm is 0.40. The saturated fractional OD change is given by exp($-S_m$) which is the Franck−Condon factor for the zero-phonon line. For a change of 0.40, $S_m = 0.9$ which is close to the value of 0.8. That the value of $S_m = 0.8$ obtained is higher than the value of 0.5 reported by Reddy et al.[15] is probably due to the lower read resolution (4 cm^{-1}) used in that work. Finally we mention that we performed a "survey" experiment in which 30 ZPH, roughly equispaced, were burned between $\sim$682 and 640 nm. The results indicate weak electron−phonon coupling, $S \lesssim 1$, for all burn wavelengths or, equivalently, all Q_y-states of the complex.

Hole-burning and Absorption Results at High Pressures. The dependence of the 77 K Q_y-absorption spectrum of LHC II on pressure up to 463 MPa was studied. The spectra for several pressures are shown in Figure 5. The red shifting of the major bands at 650, 671, and 676 nm with increasing pressure is apparent as is the larger shift rate for the 671 nm band relative to the 676 nm band that leads to an interesting narrowing of the overall absorption profile that encompasses the 671 and 676 nm bands. It should also be noted that the absorption at $\sim$662 nm decreases with increasing pressure to the point where the valley between the 650 and 671 nm bands is flat. From previous pressure dependent studies of photosynthetic complexes,[25,26,54] as well as those of isolated chromophores in polymers and glasses, which are discussed in those works, one expects that the rates of shifting seen in Figure 5 should depend linearly on the pressure. Figure 6 confirms this expectation; the linear shift rates for the 650, 671, and 676 bands are -0.088, -0.094, and -0.069 cm^{-1}/MPa, respectively. Since these bands are contributed to by several states, the pressure shifts should be viewed as averages. Higher selectivity is achieved using hole burning. The upper and lower data points in Figure 7 are for ZPH burned at 12 K with $\lambda_B = 677$ and 678 nm, respectively. These wavelengths are close to the maximum of the ZPH action spectrum of Figure 2. The linear shift rates of -0.077 and -0.088 cm^{-1}/MPa at 4.2 K are similar to those given above. For a better comparison with the 77 K rates, the 12 K rates should be increased by $\sim$10−15% to account for a weak dependence of the protein compressibility on temperature in that range.[26,64] The above shift rates are summarized in Table 1 where they are compared with those for other photosynthetic complexes.

TABLE 1: Linear Pressure Shifts

complex	band/state (nm)	pressure shift (cm^{-1}/MPa)
Rps. viridis RC[a]	P960	−0.42
PS II RC[b]	P680	−0.07
Cb. tepidum FMO[c]	B824	−0.10
	B800	−0.09
Rps. acidophila LH2[d]	B850	−0.39
	B870[g]	−0.51
	B800	−0.15
Rb. sphaeroides LH2[e]	B850	−0.38
	B870	−0.54
Rb. sphaeroides LH1[f]	B875	−0.63
	B896[h]	−0.67
	LHC II Trimer	
	650	−0.088
	671	−0.094
	676	−0.069
	$\sim$678	−0.077/−0.088

[a] Pressure shift from ref 26. [b] Pressure shift from ref 54. [c] Pressure shift from ref 68. [d] Pressure shift from ref 34. [e] Pressure shift from ref 34. [f] Pressure shift from ref 25. [g] Lowest energy exciton level of B850 ring. [h] Lowest energy exciton level of B875 ring. Pressure shifts for $\pi\pi^*$ states of chromophores isolated in glasses and polymer are typically in the -0.05 to -0.015 cm^{-1}/MPa range.

In the following section it is argued that the excitonic interactions of LHC II are too weak to affect the shift rates, i.e., the rates appear to be dictated by protein−Chl interactions.

4. Discussion

Assignment of the Lowest Energy State(s). With 12 Chl molecules per subunit the LHC II trimer possesses 36 Q_y-states. For perfect C_3 symmetry, i.e., no energy disorder from structural heterogeneity, there are twelve doubly degenerate states of E symmetry and twelve nondegenerate states of A symmetry. However, the absorption bands are inhomogeneously broadened and, thus, energy disorder exists and can be expected to split the degeneracies of the E levels and mix levels of A and E symmetries. As mentioned, the states associated with the 676 and 671 nm bands, Figure 1, are mainly Chl *a* in character while those associated with the 650 nm band are mainly Chl *b* in character.

The ZPH action spectrum of Figure 2 reflects the inhomogeneously broadened zero-phonon absorption profile of the lowest energy states near 680 nm. The burn fluence dependence of hole 1 obtained with excitation into higher energy bands (frames A, B, and C of Figure 3) indicates that the lowest energy state is located at 679.8 nm. As such it would be the fluorescent state at liquid helium temperatures which means that, with our values of $S_m = 0.8$ and $\omega_m = 18$ cm^{-1}, the fluorescence origin band should be displaced by $S_m\omega_m = 14$ cm^{-1} (0.61 nm) to the red of 679.8 nm, i.e., located at 680.4 nm. The nonline narrowed fluorescence spectrum obtained at 5 K is shown in Figure 8. The origin band lies at (680.3 ± 0.2) nm, in perfect agreement with the predicted value. If the lowest energy state was at 678.2 nm, the maximum of the ZPH action spectrum, the predicted position of the origin band would be 678.8 nm. On the basis of the results shown in Figure 3, it was suggested that there is another state(s) lying near 678 nm. To consider the nature of the $\sim$678 and 679.8 nm states an estimate of their percentage contribution to the Q_y-absorption spectrum is required. As found in ref 15, the low energy side of the 676 nm absorption band tails more slowly than a Gaussian. It is reasonable to assume that the deviation from Gaussian behavior is due to the 678 and 679.8 nm states. To proceed further we assumed that the combined absorption profile of these states is the profile of the

ZPH action spectrum centered at 678.2 nm and with a Gaussian width of 85 cm^{-1}. An additional constraint was imposed by the electron−phonon coupling analysis (vide supra), i.e., the fractional depth of a saturated hole is given by $\exp(-S_m)$. An upper limit for the Huang−Rhys factor S of 0.9 was estimated from a saturated hole depth of 0.40 at 681 nm assuming that the absorption due to the 676 nm band is negligible at this wavelength. Near the center of the ZPH action spectrum at 678 nm, however, a saturated hole depth of 0.24 was obtained. With the aforementioned Huang−Rhys factor of 0.9 the expression $\exp(-S_m)$ indicates that the lowest state(s) contributes only by about 60% to the full absorption at 678 nm, see shaded Gaussian profile in Figure 2. On the basis of the 4.2 K absorption spectrum truncated at 640 nm, a value of 9% is calculated for the contribution of the lowest energy state(s) to the total Q_y-absorption. Subtraction of the absorption due to the 678 and 679.8 nm states from the experimental absorption spectrum yielded a Gaussian shape for the low energy side of the 676 nm band with a fwhm of 85 cm^{-1}, see profile to the immediate left of the shaded profile in Figure 2. The above percentage of 9 corresponds to absorption by 3.2 Chl molecules of the trimer or 2.5 Chl *a* (∼0.8 Chl *a* per subunit) molecules when the integration of the absorption band is cut off at 657 nm (λ = 657 nm is judged to be a reasonable demarcation between the major regions of Chl *a* and *b* absorption, according to the assignment of Kühlbrandt et al.[6] Fifteen Chl *b* and twenty-one Chl *a* per LHC II trimer were taken into account). From the integrated absorption of both regions a ratio of the Chl *a* to Chl *b* dipole strengths of ∼2.1 is obtained which is slightly higher than the value of 1.64 reported from absorption spectra of Chl *a* and Chl *b* dissolved in ether[65] (vide infra). Excitonic calculations led to a value of 12 for the percentage absorption due to the lowest energy state of the *subunit*.[19,21,22] Consideration of only the subunit in that work appears to be justified since the shortest distance between Chl molecules belonging to different subunits is ∼20 Å with coupling energies estimated to be $\lesssim$5 cm^{-1}, much smaller than the inhomogeneous broadening of the absorption bands. The percentage of 12 corresponds to ∼1.4 Chl molecules or 1.1 Chl *a* (with a ratio of Chl *a* to Chl *b* dipole strengths of ∼2.1) molecules per subunit. The calculations reveal that while the excitonic interactions have only a weak effect on the state energies, they have a significant effect on their oscillator strengths. For illustrative purposes we consider a Chl *b*/*a* pair with a zeroth-order energy gap ΔE = 600 cm^{-1} and a coupling energy $|V|$ = 100 cm^{-1} for parallel or antiparallel alignment of the transition dipoles $\mathbf{D}_a^0$ and $\mathbf{D}_b^0$. The dipole strength correction to first order is

$$|\mathbf{D}_b|^2 = |\mathbf{D}_b^{(0)}|^2 + \left(\frac{2V}{\Delta E}\right)\mathbf{D}_a^{(0)}\cdot\mathbf{D}_b^{(0)} \qquad (1)$$

for the higher energy state associated mainly with Chl *b* and

$$|\mathbf{D}_a|^2 = |\mathbf{D}_a^{(0)}|^2 - \left(\frac{2V}{\Delta E}\right)\mathbf{D}_a^{(0)}\cdot\mathbf{D}_b^{(0)} \qquad (2)$$

for the state associated mainly with Chl *a*. Using the usual expression for the dipole−dipole interaction it follows that the cross terms in (1) and (2) are negative and positive, respectively, for the in-line alignment of $\mathbf{D}_a^0$ and $\mathbf{D}_b^0$. For the sandwich alignment the reverse is true. To fit the absorption spectrum it was found that in-line alignments are required.[21] For $|\mathbf{D}_a^{(0)}|^2/|\mathbf{D}_b^{(0)}|^2$ = 1.6,[65] $|\mathbf{D}_a|^2/|\mathbf{D}_b|^2$ = 3.6 for our model pair, i.e., the effect on the oscillator strengths is rather large and readily explains our finding of an average ratio of Chl *a* to Chl *b* dipole strengths of ∼2.1. On the other hand, the occupation numbers of Chl *a* for the upper state and of Chl *b* for the lower state are only ∼0.03. (The magnitude of the second-order energy corrections is 17 cm^{-1}). The above example reveals the essential physics responsible for the result from the excitonic calculations that the lowest energy state of the subunit carries the dipole strength of 1.1 Chl *a* molecules even though from an occupation number point of view the state is highly localized on a single Chl *a* (Chl *a* no. 5 according to the labeling of Kühlbrandt et al.[6]). The calculations predict that all states of the subunit are quite highly localized on a single Chl molecule. We hasten to add that our determination of 0.8 Chl *a* molecules per subunit is not accurate enough to exclude a somewhat higher (or lower) value. The Gaussian profile of the 676 nm band shown in Figure 2 carries twice the intensity of the profile of the ∼680 nm band and, therefore, has the absorption strength of approximately five Chl *a* molecules. The remainder of the absorption for λ > 657 nm is then equivalent to that of ∼13.5 Chl *a* molecules.

In view of the above results and discussion, it is reasonable to conclude that the 679.8 and ∼678 nm states stem from the lowest energy and monomer-like state of the subunit. Within this picture there would be three states in the trimer which are expected to be degenerate in the absence of intersubunit interactions and energy disorder due to structural heterogeneity. In the presence of both, the degeneracy would be removed and for an ensemble of LHC II trimers the 679.8 nm state would lie lowest in energy. This means that there would need to be two nondegenerate (on average) states absorbing near 678 nm which are not resolved in the hole-burned spectra. This seems reasonable since we found that the envelope of the ZPH spectrum shown in Figure 2 with a width of 85 cm^{-1} can be fitted with three Gaussians of equal width (70 cm^{-1}) and intensity centered at 679.8, 678.4, and 677.1 nm. The width of 70 cm^{-1} was chosen because it is the width of the 679.8 nm hole shown in frame C of Figure 3. The splitting between the upper two levels and lower two levels is ∼30 cm^{-1}. The three states should be quite highly localized on individual subunits for an intersubunit Chl *a*-Chl *a* coupling $\lesssim$5 cm^{-1} and an energy inequivalence of 30 cm^{-1}.[41]

Chl−Chl Coupling Strengths. In simplest terms the mechanism of NPHB involves a more or less persistent structural change of the chromophore−host matrix system that is triggered by electronic excitation.[66] For a system of excitonically coupled chromophores such as found in photosynthetic complexes, the responses of excited states other than the one in which NPHB occurs can be used to gauge the extent of excitonic delocalization. The responses appear as persistent satellite holes. The reaction center of *Rhodopseudomonas viridis* provides the clearest example of this. Nonphotochemical hole burning of the lowest energy Q_y-state (P_-) of the special pair of BChl *b* molecules elicits an appropriately large response of the upper special pair state (P_+) which is manifest as an intense hole in the P_+ absorption band.[53] In fact, the satellite hole structure was used to definitively assign the absorption band of P_+ and to assess the extent to which the special pair contributes to bands associated with other cofactors. Another good example is the FMO complex of *P. aestuarii*.[47] As can be seen from the spectra of Figures 1 and 4, hole burning of the absorption due to the lowest energy states (hole 1) results in only weak satellite holes associated with the higher energy absorption bands (see, e.g., hole 2 at ∼648 nm). It appears, therefore, that the Chl *a* molecule of the subunit associated with the ∼680 nm states is weakly coupled to the Chl *b* molecules responsible for the 650 nm band, in agreement with the preliminary assignment of Chl

a and *b* molecules[6] and excitonic calculations[19,22] which reveal that the largest interaction energies can be expected within Chl *b*/*a* dimers. This conclusion is further consistent with the results of femtosecond experiments (12 K) which show that subpicosecond Chl *b* → Chl *a* does not occur directly to the 680 nm states. Rather, population of these states occurs on a time scale of tens of picoseconds following EET to states associated with the 671 and 676 nm bands.[10,11] There is very little satellite hole activity between ~650 and 671 nm. Unfortunately, the antihole of hole 1 marked with an asterisk in Figure 1 interferes with the satellite hole of the 676 nm band and, to a less extent, that of the 671 nm band. The satellite hole of the latter band, which is indicated by the arrow in Figure 4, is clearly weak relative to hole 1. On the basis of the results of Figure 4 we estimate that the Δ-absorbance value for the satellite hole of the 676 nm band is no more than about a factor of 2 greater than that of the 671 nm band satellite hole. In summary, the weak satellite hole structure produced by hole burning of the lowest energy states of the LHC II trimer, which appear to be associated mainly with a single Chl *a* molecule of the subunit, indicate that this Chl *a* molecule is weakly coupled to others of the subunit. In fact, the satellite hole structure is so weak that a contribution to the satellite structure from another mechanism might be considered. It is that the protein structural change that accompanies NPHB is not confined to the immediate region around the excited Chl *a* molecule but is spatially extended to the extent that the transition frequencies of other Chl molecules are altered.

Recently, high pressure has been combined with low-temperature absorption and hole-burning spectroscopies in order to assess the strength of excitonic couplings in photosynthetic complexes.[25,26] Some of the linear pressure shift rates obtained for absorption bands and states (via hole burning) of several complexes are given in the upper part of Table 1. The shift rates from this work on the LHC II trimer are listed at the bottom. As reviewed in refs 25 and 26, shift rates have been determined by other groups using hole burning for the S_1 $\pi\pi^*$ states of chromophores *isolated* in glass, polymer, and protein hosts. They lie in the range of −0.05 to −0.15 cm^{-1}/MPa. The theory of Laird and Skinner[67] has been used with the shift rates to estimate the isotropic compressibilities (κ). Typical values for glasses and proteins are close to 0.1 GPa^{1-}. As discussed in refs 25 and 54, a shift rate greater than ~0.2 cm^{-1}/MPa for a photosynthetic complex indicates that excitonic interactions are sufficiently strong for their pressure dependence to make a contribution to the rate. That is, the protein−Chl interactions are not the dominant factor. It is instructive to consider the very large shift rates observed for the B850 absorption band and the lowest exciton level (B870) of the B850 ring of the LH2 complex as well as the B875 band and lowest exciton level (B896) of the B875 ring of the LH1 complex. Although the nearest neighbor Coulombic BChl *a*−BChl *a* couplings are large, ~400 cm^{-1} at cryogenic temperatures, the theoretical analysis given in ref 25 showed that these couplings contribute only ~ −0.1 cm^{-1}/MPa to the shift rate. With the addition of another − 0.1 cm^{-1}/MPa from protein-BChl interactions one still falls far short of the observed rates. The shortfall for B896 is ~ −0.4 cm^{-1}/MPa. Further analysis revealed that the shortfalls can be understood in terms of electron-exchange interactions.[25] It should be noted that the nearest interatomic distances between BChl *a* molecules are ~3.5 Å, short enough to suggest that electron-exchange could be important. The shortest $R_{Mg\cdots Mg}$ distances are close to 9 Å, comparable to the shortest Chl *b*−Chl *a* distances of LHC II. Although the shortest Chl *b*−Chl *a* interatomic distances reported in ref 6 are 4.0 Å, there is considerable uncertainty in that value given the limited resolution. Thus, the possibility exists that electron-exchange coupling between Chl *a* and *b* molecules could be of some importance.

To explore this possibility and others it is useful to reduce the theoretical analysis given in ref 25 for the B850 and B875 antenna rings of purple bacteria to the case of a heterodimer. By necessity we also assume that the complexes are isotropic with a bulk compressibility of κ. As before, $\Delta E > 0$ is the zeroth-order splitting between the monomers of the heterodimer and V is the monomer−monomer coupling energy. We will assume, as appears to be the case for the Chl *a*/*b* pairs of LHC II, that V is sufficiently small relative to ΔE to permit the use of second-order perturbation theory to evaluate the contribution from V to the energies of the two heterodimer states. The fractional change in the intermonomer distance R for a pressure increase of ΔP is

$$\left|\frac{\Delta R}{R}\right| = 3^{-1}\kappa\Delta P \tag{3}$$

For $\kappa = 0.1$ GPa^{1-} and $\Delta P = 1$ GPa (greater than achievable with our apparatus), the fractional change is only 0.03. Thus for $R = 9$ Å, $\Delta R = 0.3$ Å. For the case of dipole−dipole (dd) coupling, the pressure shift rate is given by

$$\left|\left(\frac{\partial\nu}{\partial P}\right)_{dd}\right| = \left|\left(\frac{2V_{dd}}{\Delta E}\right)(\kappa\, V_{dd})\right| \tag{4}$$

where we have made the reasonable assumption that the dependence of ΔE on P due to interactions with the protein is negligible. The upper and lower heterodimer levels shift to higher and lower energies, respectively. For a Chl *a*−Chl *b* interaction of $V_{dd} = 100$ cm^{-1}, $\kappa = 0.1$ GPa^{1-} (vide supra), and $\Delta E = 600$ cm^{-1}, $|(\partial\nu/\partial P)_{dd}| = 0.003$ cm^{-1}/MPa, which is insignificant. The pressure shift for a homodimer is obtained by setting $2V/\Delta E$ in eq 4 equal to unity. Even for this case, the pressure shift rate is low, 0.01 cm^{-1}/MPa.

For the case of electron-exchange (CT) coupling

$$\left|\left(\frac{\partial\nu}{\partial P}\right)_{CT}\right| = \left|\left(\frac{2V_{CT}}{\Delta E}\right)(3^{-1}\kappa A\, R_{CT})\right| \tag{5}$$

where R_{CT} is the ambient pressure value for the relevant interatomic distance associated with the CT coordinate and A is a constant dependent on the system. For B870 and B896 the pressure shift rates led to $A \sim 85$ and 125 cm^{-1}/0.1 Å, respectively, for $R = 3.5$ Å. If for a Chl *a*/*b* pair of LHC II we take $R_{CT} = 3.5$ Å, $V_{CT} = 100$ cm^{-1} and $A = 100$ cm^{-1}/0.1 Å, the shift rate from eq 5 is 0.04 cm^{-1}/MPa, which is significant and comparable to the observed rates (Table 1), but we emphasize that the value of A used represents a sizable electron-exchange coupling. The sign of the shift rate for the upper and lower heterodimer levels is positive and negative, respectively, so that their rates would add destructively and constructively to the expected negative shift rate from protein−Chl interactions. However, the observed shift rate for the 650 nm band is nearly the same as those for the 671 and 676 nm bands, indicating that A is smaller than 100 cm^{-1}/0.1 Å especially when it is considered that three Chl *a*/*b* pairs may contribute to the 650 nm band. Again, the estimated dipole−dipole Chl *a*/*b* coupling energies are too small to contribute significantly to the shift rates. Given that the nearest Chl *a*−Chl *a* and Chl *b*−Chl *b* distances appear to be no shorter than 11 Å,[22] it is likely that

TABLE 2: Zero-Phonon Holewidths and Dephasing Times

	4.2 K/λ_B (nm)							
	675.0	676.0	677.0	678.0	679.0	680.0	681.0	682.0
$\Delta A/A$[a]	0.02	0.03	0.07	0.12	0.16	0.17	0.17	0.13
Γ_{hole} (cm^{-1})[b]	2.0 ± 0.4	1.7 ± 0.4	1.2 ± 0.3	0.8 ± 0.2	0.7 ± 0.2	0.5 ± 0.1	0.5 ± 0.1	0.5 ± 0.1
Γ_{hom} (cm^{-1})[c]	0.9 ± 0.2	0.7 ± 0.2	0.5 ± 0.2	0.3 ± 0.1	0.2 ± 0.1	0.1	0.1	0.1
T_2 (ps)[d]	12 ± 3	15 ± 5	20 ± 10	40 ± 10	~100	*e*	*e*	*e*

[a] Fractional absorbance change of hole. [b] Measured holewidth, uncorrected for read resolution of 0.3 cm^{-1}. [c] Homogeneous width of zero-phonon line, corrected for read resolution. [d] Total optical dephasing time, $(\pi\ \Gamma_{hom}\ c)^{-1}$. [e] Resolution inadequate for determination.

the associated excitonic interactions are of little importance for understanding the pressure shifts. That the shift rate of ~ -0.08 cm^{-1}/MPa for the lowest state(s) near 680 nm is nearly the same as the shift rates for the higher states is consistent with it being dominated by a single Chl *a* molecule of the subunit that is weakly coupled to others. We note that excitonic interactions for pressure shifting are also of minimal importance[68] for the FMO BChl *a* antenna complex which features Coulombic BChl *a*−BChl *a* couplings as large as ~150 cm^{-1}, as well as[54] the special pair, P680, of the PS II RC with an apparent Chl *a*−Chl *a* coupling of ~150 cm^{-1}; see Table 1 for the "monomer-like" shift rates. That the shift rates for B800 of the LH2 complex fall in the monomer range is consistent with the large separation distance (~21 Å) and concomitant weak coupling (~25 cm^{-1}) between neighboring BChl *a* molecules of the B800 ring.[34]

To conclude this section we note that upon raising the pressure to 425 MPa an increase of oscillator strength of ~5% was observed for the Chl *a* region (integrated for $\lambda > 657$ nm) as might be expected based on excitonic calculations of Renger et al.[21,22] Nevertheless, the excitonic interactions of LHC II appear to be too weak to affect the shift rates, i.e., the rates seem to be dictated by protein−Chl interactions.

Excitation Energy Transfer and Optical Dynamics. We consider first the widths of holes burned with wavelengths near the maximum of the 650 nm band, Figure 1. As pointed out, for λ_B-values to lower energy of the 650 nm band a broad hole with a width of ~125 cm^{-1} is produced with a maximum slightly to the blue of the 650 nm band's maximum. The bottom two hole spectra (b and c) of Figure 1 show examples of this. For such λ_B-values the width of 125 cm^{-1} for hole 2 carries no dynamical information since the SDF of the state(s) excited are uncorrelated with those of the states associated with the 650 nm band. The situation is different when λ_B is located within the 650 nm band site since, now, one is site excitation energy selective for that band. The top hole-burned spectrum a of Figure 1 was obtained with $\lambda_B = 648.6$ nm. One can observe a broad hole analogous to hole 2 with a relatively sharp ZPH with a width of ~8 cm^{-1} superimposed on it. Similar spectra were obtained for several burn wavelengths between 648 and 651 nm. From these spectra it was determined that the widths of the relatively sharp ZPH coincident with λ_B fall in the range of 7−8 cm^{-1} while the widths of the broad hole are about 125 cm^{-1}. (Since the fractional absorbance changes of these holes are small, $\lesssim 0.01$, we can be no more precise.) It is reasonable to associate the ~8 cm^{-1} width with energy transfer from a mainly Chl *b* state to lower energy states. Since the ZPH width (Γ_{hole}) is twice the width of the ZPL (Γ_{hom}), the energy transfer time is given by $[2\pi(2^{-1}\Gamma_{hole})c]^{-1}$, where c is the speed of light, 3×10^8 cm s^{-1}. For $\Gamma_{hole} = 8$ cm^{-1}, the transfer time is ~1 ps. We suggest that this transfer time corresponds to the ≈600 fs component observed in femtosecond experiments, cf. Introduction. The broad hole with a width of ~125 cm^{-1} is especially interesting. Since 125 cm^{-1} is comparable to the width of the 650 nm absorption band, the relationship $\Gamma_{hole} = 2\ \Gamma_{hom}$ breaks down and $\Gamma_{hole} \approx \Gamma_{hom}$.[47] The 125 cm^{-1} holewidth then yields a transfer time of ≈40 fs which is a factor of about 4 shorter than the fastest transfer time from Chl *b* states measured by femtosecond spectroscopy. This discrepancy begs some interpretation. To this end we note first that since the 650 nm band is contributed to by more than one state, the 125 cm^{-1} hole could be the superposition of two unresolved holes. This would reduce the discrepancy by about a factor of 2. Second, it is likely that the states pumped with our CW laser are different than the state created with a femtosecond pulse, a state that is a coherent superposition of eigenstates that underlie the frequency profile of the pulse. The energy transfer dynamics would be expected to be different if dephasing of the superposition state was not complete prior to Chl *b* → Chl *a* transfer.

We consider now the widths of the ZPH associated with the action spectrum of Figure 2. Table 2 lists the fractional absorbance changes and widths (Γ_{hole}) of eight holes read with a resolution of 0.3 cm^{-1}. The third row lists the homogeneous widths of the ZPLs obtained using $\Gamma_{hom} = (\Gamma_{hole} - 0.3)/2$ which probably overcorrects for the read resolution. Γ_{hom} is constant for $\lambda_B \gtrsim 679.0$ nm and increases for $\lambda_B \lesssim 679.0$ nm. Since the fractional ΔA-values are lower than 0.1 for the 675.0, 676.0, and 677.0 nm holes, it is unlikely that their widths are significantly contributed to by saturation broadening.[62] In addition, the contribution from pure dephasing due to phonons and two-level systems (TLS) of the protein should be negligible, vide infra. Therefore, we attribute the Γ_{hom}-values for these three holes to EET. The corresponding total dephasing times (T_2) are 12, 15, and 20 ps, respectively, Table 2. The T_1 lifetimes are ~6, 8, and 10 ps since $T_2 = 2\ T_1$. The T_1 lifetimes are in good agreement with the values reported by Savikhin et al.[8] at 13 K on the basis of pump−probe anisotropy decays at 675 and 677 nm. We attribute the T_1 lifetimes to downward EET from states associated with the 676 nm band although for $\lambda_B = 677$ nm the possibility of intersubunit EET from the subunit with the highest energy for the lowest state to the 678.4 and 679.8 nm states of the other two subunits, vide supra, cannot be excluded.

Turning to the $\lambda_B = 679.0-682.0$ nm ZPHs it is apparent from Table 2 that the read resolution of 0.3 cm^{-1} is too low to permit determination of the T_2-values. Furthermore, the fractional ΔA-values are > 0.1 so that the holes may be contaminated by some saturation broadening.[62] Since we have proven that the 679.8 nm state is the lowest and the fluorescent (at 4.2 K) state of the trimer, its T_1-value should be ~5.6 ns,[51] which corresponds to Γ_{hom} ~0.001 cm^{-1} in the absence of pure dephasing. Our recent finding[69] that the optical dynamics for T ≲ 15 K of the lowest energy exciton level of the B850 and B875 BChl *a* antenna rings of purple bacteria are dictated by pure dephasing (spectral diffusion) due to the glasslike TLS of the protein suggests that such dephasing may be important for the 679.8 nm state. High resolution (≲20 MHz for burning and reading) experiments are planned to investigate, in detail, this possibility for a wide range of λ_B-values. At this time, however,

we can present preliminary results that establish that dephasing due to TLS is operative. Holes were burned ($\Delta A/A < 0.1$) and read at 1.9, 4.7, 5.2, 6.1, 7.8, 9.2, and 10.1 K with λ_B-values in the 681−682 nm region. The width of the hole followed a $T^{1.3\pm0.1}$ temperature dependence which is the signature for TLS-induced dephasing/spectral diffusion.[56] For example, $\Gamma_{hom} = 0.037$, 0.073 and 0.30 cm^{-1} for $T = 1.9$, 4.7, and 9.2 K, respectively. It is encouraging to note that our estimated value for Γ_{hom} of 0.1 cm^{-1} for 4.2 K is comparable to the value of 0.073 cm^{-1} at 4.7 K.

Acknowledgment. Research at the Ames Laboratory was supported by the Division of Chemical Sciences, Office of Basic Energy Sciences, U.S. Department of Energy. Ames Laboratory is operated for USDOE by Iowa State University under Contract W-7405-Eng-82. J.P. greatfully acknowledges support from the International Institute of Theoretical and Applied Physics (IITAP) in Ames. Research in Berlin was supported by NAFöG and the German Academic Exchange Service (DAAD). K.-D.I., J.V., and G.R. acknowledge financial support by Deutsche Forschungsgemeinschaft (Grants SFB 312, TP A2, and A6).

References and Notes

(1) Renger, G. In *Topics in Photosynthesis*; Barber, J., Ed.; Elsevier: Amsterdam, 1992; p 45.
(2) van Grondelle, R.; Dekker: J. P.; Gillbro, T.; Sundstrom, V. *Biochim. Biophys. Acta* **1994**, *1187*, 1.
(3) Sundström, V.; van Grondelle, R. In *Anoxygenic Photosynthetic Bacteria*; Blankenship, R. E., Madigan, M. T., Baller, C. E., Eds.; Kluwer Academic Publishers: Dordrecht, 1995; p 349.
(4) Freiberg, A. In *Anoxygenic Photosynthetic Bacteria*; Blankenship, R. E., Madigan, M. T., Baller, C. E., Eds.; Kluwer Academic Publishers: Dordrecht, 1995; p 385.
(5) Jansson, S. *Biochim. Biophys. Acta* **1994**, *1184*, 1.
(6) Kühlbrandt, W.; Wang, D. N.; Fujiyoshi, Y. *Nature* **1994**, *367*, 614.
(7) Connelly, J. P.; Müller, M. G.; Hucke, M.; Gatzen, G.; Mullineaux, C. W.; Ruban, A. V.; Horton, P.; Holzwarth A. R. *J. Phys. Chem. B* **1997**, *101*, 1902.
(8) Savikhin, S.; van Amerongen, H.; Kwa, S. L. S.; van Grondelle, R.; Struve, W. S. *Biophys. J.* **1994**, *66*, 1597.
(9) Du, M.; Xie, X.; Mets, L.; Fleming, G. R. *J. Phys. Chem.* **1994**, *98*, 4736.
(10) Bittner, T.; Irrgang, K.-D.; Renger, G.; Wasilewski, M. R. *J. Phys. Chem.* **1994**, *98*, 11821.
(11) Bittner, T.; Wiederrecht, G. P.; Irrgang, K.-D.; Renger, G.; Wasilewski, M. R. *Chem. Phys.* **1995**, *194*, 311.
(12) Visser, H. M.; Kleima, F. J.; van Stokkum, I. H. M.; van Grondelle, R.; van Amerongen, H. *Chem. Phys.* **1996**, *210*, 297.
(13) Hemelrijk, P. W.; Kwa, S. L. S.; van Grondelle, R.; Dekker: J. P. *Biochim. Biophys. Acta* **1992**, *1098*, 159−166.
(14) Kwa, S. L. S.; Groeneveld, F. G.; Dekker: J. P.; van Grondelle, R.; van Amerongen, H.; Lin, S.; Struve, W. S. *Biochim. Biophys. Acta* **1992**, *1101*, 143.
(15) Reddy, N. R. S.; van Amerongen, H.; Kwa, S. L. S.; van Grondelle, R.; Small, G. J. *J. Phys. Chem.* **1994**, *98*, 4729.
(16) Peterman, E. J. G.; Pullerits, T.; van Grondelle, R.; van Amerongen, H. *J. Phys. Chem. B* **1997**, *101*, 4448.
(17) Peterman, E. J. G.; Dukker, F. M.; van Grondelle, R.; van Amerongen, H. *Biochim. Biophys. Acta* **1992**, *69*, 2670.
(18) Kleima, F. J.; Gradinaru, C. C.; Calkoen, F.; van Stockum, I. H. M.; van Grondelle, R. *Biochemistry* **1997**, *36*, 15262.
(19) Voigt, J.; Renger, Th.; Schödel, R.; Schrötter, T.; Pieper, J.; Redlin, H. *Phys. Status Solidi B* **1995**, *194*, 333.
(20) Gülen, D.; van Grondelle, R.; van Amerongen, H. In *Photosynthesis: From Light to Biosphere*, Proceedings of the 10th International Photosynthesis Conference; Mathis, P., Ed.; Kluwer Academic Publishers: Dordrecht, 1995; Vol. 1, p 335.
(21) Renger, Th.; Voigt, J.; May, V.; Kühn, O. *J. Phys. Chem. B* **1997**, *100*, 15654.
(22) Renger, Th. Ph.D. Thesis, Humboldt-University, Berlin, 1995.
(23) Trinkunas, G.; Conelly, J. P.; Müller, M. G.; Valkunas, L.; Holzwarth, A. R. *J. Phys. Chem. B* **1997**, *101*, 7313.
(24) Pieper, J.; Irrgang, K.-D.; Rätsep, M.; Jankowiak, R.; Schrötter, Th.; Voigt, J.; Small, G. J.; Renger, G. *J. Phys. Chem. B* **1999**, xxx, xxxxx.
(25) Wu, H.-M.; Rätsep, M.; Jankowiak, R.; Cogdell, R. J.; Small, G. J. *J. Phys. Chem. B* **1998**, *102*, 4023.
(26) Reddy, N. R. S.; Wu, H.-M.; Jankowiak, R.; Picorel, R.; Cogdell, R. J.; Small, G. J. *Photosyn. Res.* **1996**, *48*, 277.
(27) Johnson, S. G.; Lee, I.-J.; Small, G. J. In *Chlorophylls*; Scheer, H., Ed.; CRC Press: Boca Raton, 1991; p 739.
(28) Reddy, N. R. S.; Lyle, P. A.; Small, G. J. *Photosyn. Res.* **1992**, *31*, 167.
(29) Bradforth, S. E.; Jimenez, R.; van Mourik, F.; van Grondelle, R.; Fleming, G. R. *J. Phys. Chem.* **1995**, *99*, 16179.
(30) Visser, H. M.; Somsen, O. J. G.; van Mourik, F.; van Grondelle, R. *J. Phys. Chem. B* **1997**, *100*, 18859.
(31) Peloquin, J. M.; Lin, S.; Taguchi, A. K. W.; Woodbury, N. W. *J. Phys. Chem.* **1995**, *99*, 1349.
(32) Kolaczkowski, S. V.; Hayes, J. M.; Small, G. J. *J. Phys. Chem.* **1994**, *98*, 13418.
(33) Mukamel, S. *Principles of Nonlinear Spectroscopy*; Oxford University Press: New York, 1995.
(34) Wu, H.-M.; Rätsep, M.; Jankowiak, R.; Cogdell, R. J.; Small, G. J. *J. Phys. Chem. B* **1997**, *101*, 7641.
(35) Wu, H.-M.; Reddy, N. R. S.; Cogdell, R. G.; Muenke, C.; Michel, H.; Small, G. J. *Mol. Cryst. Liq. Cryst.* **1996**, *291*, 163.
(36) Gudowska-Nowak, E.; Newton, M. D.; Fajer, J. *J. Phys. Chem.* **1990**, *94*, 5795.
(37) Reddy, N. R. S.; Picorel, R.; Small, G. J. *J. Phys. Chem.* **1992**, *96*, 6458.
(38) Davydov, A. S. *Theory of Molecular Excitons*; Plenum Press: New York, 1971.
(39) Alden, R. G.; Johnson, E.; Nagarjan, V.; Parson, W. W.; Law, C.; Cogdell, R. G. *J. Phys. Chem. B* **1997**, *101*, 4667.
(40) Wu, H.-M.; Small, G. J. *Chem. Phys.* **1997**, *218*, 225.
(41) Wu, H.-M.; Small, G. J. *J. Phys. Chem. B* **1998**, *102*, 888.
(42) Fenna, R. E.; Matthews, B. W. *Nature* **1975**, *258*, 573.
(43) Li, Y.-F.; Zhou, W.; Blankenship, R. E.; Allen, J. P. *J. Mol. Biol.* **1997**, *271*, 456.
(44) Rätsep, M.; Wu, H.-M.; Hayes, J. M.; Blankenship, R. E.; Cogdell, R. J.; Small, G. J. *J. Phys. Chem. B* **1998**, *102*, 4035.
(45) Louwe, R. J. W.; Vrieze, J.; Hoff, A. J.; Aartsma, T. J. *J. Phys. Chem. B* **1997**, *101*, 11280.
(46) Savikhin, S.; Buck, D. R.; Struve, W. S. *J. Phys. Chem. B* **1999**. In press
(47) Johnson, S. G.; Small, G. J. *J. Phys. Chem.* **1991**, *95*, 471.
(48) Irrgang, K.-D.; Boekema, E. J.; Vater, J.; Renger, G. *Eur. J. Biochem.* **1988**, *178*, 209.
(49) Peterman, E. J. G.; Hobe, S.; Calkoen, F.; van Grondelle, R.; Paulsen, H.; van Amerongen, H. *Biochim. Biophys. Acta* **1996**, *1273*, 171.
(50) Porra, R. G.; Thompson, W. A.; Kriedemann, P. E. *Biochim. Biophys. Acta* **1989**, *975*, 384.
(51) Vasiliev, S.; Irrgang, K.-D.; Schrötter, T.; Bergmann, A.; Eichler, H.-J.; Renger, G. *Biochemistry* **1997**, *36*, 7503.
(52) Vasiliev, S.; Schrötter, T.; Bergmann, A.; Irrgang, K.-D.; Eichler, H.-J.; Renger, G. *Photosynthetica* **1996**, *33*, 553.
(53) Reddy, N. R. S.; Kolaczkowski, S. V.; Small, G. J. *J. Phys. Chem.* **1993**, *97*, 6934.
(54) Chang, H. C.; Jankowiak, R.; Reddy, N. R. S.; Small, G. J. *Chem. Phys.* **1995**, *197*, 307.
(55) Reddy, N. R. S.; Small, G. J. In *Biophysical Techniques in Photosynthesis*; Amesz, J., Hoff, A. J., Eds.; Kluwer Academic Publishers: Dordrecht, 1996; p 123.
(56) Völker, S. In *Relaxation Processes in Molecular Excited States*; Fünfschilling, J., Ed.; Kluwer Academic Publishers: Dordrecht, 1989; p 113.
(57) Hayes, J. M.; Jankowiak, R.; Small, G. J. In *Persistent Spectral Hole-Burning: Science and Applications*; Moerner, W., Ed.; Springer-Verlag: Berlin, 1988; p 153.
(58) Silbey, R.; Kassner, K. *J. Lumin.* **1987**, *36*, 283.
(59) Kim, W.-H.; Reinot, T.; Hayes, J. M.; Small, G. J. *J. Phys. Chem.* **1995**, *99*, 7300.
(60) Shu, L.; Small, G. J. *J. Opt. Soc. Am. B* **1990**, *9*, 724.
(61) Hayes, J. M.; Lyle, P. A.; Small, G. J. *J. Phys. Chem.* **1994**, *98*, 7337.
(62) Lee, I.; Hayes, J. M.; Small, G. J. *J. Chem. Phys.* **1989**, *91*, 3463.
(63) Lyle, P. A.; Kolaczkowski, S. V.; Small, G. J. *J. Phys. Chem.* **1993**, *97*, 6924.
(64) Perepechko, I., Ed. *Low-Temperature Properties of Polymers*; Pergamon: Oxford, 1980.
(65) Lichtenthaler, H. K. *Methods Enzymol.* **1987**, *148*, 350.
(66) Shu, L.; Small, G.J. *Chem. Phys.* **1990**, *141*, 447.
(67) Laird, B. B.; Skinner, J. L. *J. Chem. Phys.* **1989**, *90*, 3274.
(68) Reddy, N. R. S.; Jankowiak, R.; Small, G. J. *J. Phys. Chem.* **1995**, *99*, 16168.
(69) Wu, H.-M.; Rätsep, M.; Lee, I.-J.; Cogdell, R. J.; Small, G. J. *J. Phys. Chem. B* **1997**, *101*, 7654.